Environmental Science
Atmospheres

ROYAL SOCIETY
OF **CHEMISTRY**

PAPER
Eshani Hettiarachchi and Vicki H. Grassian
Heterogeneous chemistry of methyl ethyl ketone on mineral oxide surfaces: impacts of relative humidity and nitrogen dioxide on product formation

Check for updates

Heterogeneous chemistry of methyl ethyl ketone on mineral oxide surfaces: impacts of relative humidity and nitrogen dioxide on product formation†

Eshani Hettiarachchi [ID] and Vicki H. Grassian [ID] *

Despite their atmospheric abundance, heterogeneous and multiphase reactions of carbonyl compounds are poorly understood. In this study, we investigate the surface adsorption and surface chemistry of methyl ethyl ketone (MEK), the second most abundant ketone in the atmosphere, with several mineral oxide surfaces including SiO_2, α-Fe_2O_3 and TiO_2. In particular, the chemistry of MEK with these common components of mineral dust, under both dry and high relative humidity (RH%) conditions, has been investigated. Furthermore, reactions of adsorbed MEK with gas-phase NO_2 were also examined. We show that MEK molecularly and reversibly adsorbs on SiO_2 whereas irreversible adsorption occurs on both α-Fe_2O_3 and TiO_2 surfaces, followed by the formation of higher molar mass species resulting from dimerization and oligomerization reactions. Isotope labeling experiments confirmed the incorporation of H atoms from surface hydroxyl groups and strongly adsorbed water into these oligomer products. Most interesting is that at 80% RH, oligomer formation on α-Fe_2O_3 shifts toward a higher relative abundance of MEK tetramer relative to the dimer while on TiO_2 there was no change in product distribution. In the presence of gas-phase NO_2, MEK undergoes degradation to formaldehyde and acetaldehyde, followed by the formation of aldol condensation products of these aldehydes on the α-Fe_2O_3 surface. Overall, this study provides mechanistic insights on mineralogy-specific heterogeneous chemistry of a prevalent and atmospherically abundant ketone.

Environmental significance

Methyl ethyl ketone (MEK) is the second most abundant ketone in the atmosphere and an important precursor of secondary organic aerosols. Currently its reactions with primary pollutant gases and water vapor in the presence of mineral surfaces are poorly understood. Heterogeneous reactions of MEK on mineral oxide surfaces show a range of products that form on the surface in the presence of water and nitrogen dioxide and the product distribution changes. Eighteen different compounds are found suggesting multiple mechanisms by which MEK can interact with these surfaces. These results improve our understanding of heterogeneous chemistry of mineral dust aerosols and, in particular, reactions of carbonyl compounds on mineral surfaces.

1 Introduction

Secondary organic aerosols (SOAs) form a significant fraction of atmospheric particulate matter (PM) and play important roles in climate change, air quality, and human health.[1–5] Atmospheric carbonyl compounds are the major constituents of

Department of Chemistry and Biochemistry, University of California San Diego, 9500 Gilman Drive, La Jolla, California 92093, USA. E-mail: vhgrassian@ucsd.edu

† Electronic supplementary information (ESI) available: MEK gas-phase FTIR spectrum, HRMS pattern for the MEK standard, MS/MS fragmentation of identified surface products, FTIR spectra for MEK adsorption on hydroxylated and deuteroxylated α-Fe_2O_3 surfaces and peak assignments, HRMS pattern for surface products for MEK adsorption on deuteroxylated α-Fe_2O_3 and TiO_2 surfaces, mass spectrometry data of identified deuterated products, and HRMS pattern for surface products for MEK adsorption on authentic dust. See DOI: https://doi.org/10.1039/d3ea00023k

SOAs.[6–9] Low molar mass carbonyl compounds such as acetone and methyl ethyl ketone (MEK) are primary precursors contributing to numerous oxygenated SOAs.[9] For example, polymers formed from small carbonyls are a major component of organic aerosols.[10] Gas-phase photochemical reactions with atmospheric oxidants such as hydroxyl radicals and ozone are considered to be the major reaction pathways for carbonyl compounds due to their higher volatility.[6,9,11,12] Furthermore, some carbonyl compounds such as glyoxal are precursors for Brown Carbon (BrC) formation.[13–17] Despite the abundance of carbonyl compounds in the atmosphere, for the most part, heterogeneous and multiphase reactions of these compounds on mineral surfaces were considered insignificant due to their volatility.[12]

MEK is the second most abundant atmospheric carbonyl compound after acetone,[11,18] with a typical mixing ratio of 0.03–

© 2023 The Author(s). Published by the Royal Society of Chemistry

Environ. Sci.: Atmos., 2023, **3**, 799–815 | **799**

4 ppb.[19] MEK is emitted *via* both biogenic and anthropogenic sources. Biogenic sources include direct emissions such as biomass burning and from the terrestrial biosphere, including but not limited to dry plant matter, plant roots, and bacteria.[19–24] MEK is directly emitted from certain anthropogenic sources such as solvent evaporation, vehicle exhaust,[19,25–28] and secondary production from the oxidation of anthropogenic alkanes.[11,29,30] Although MEK has been detected alongside other volatile organic compounds (VOCs), atmospheric MEK has received little attention[19] and there are few studies of its heterogeneous reactions on aerosol surfaces.[31–34] Although unrelated to atmospheric chemistry, some studies on MEK adsorption on photocatalysts such as TiO_2 have found, and in the absence of light, the MEK adsorption correlates with the surface area of the catalyst.[35] In the gas phase, MEK reacts with hydroxyl radicals to form acetaldehyde and formaldehyde.[19] These carbonyl compounds although have long been considered insignificant contributors to aerosol mass due to their higher volatility, recent studies conducted with formaldehyde and glyoxal suggest otherwise.[36–39] In particular, the hydration of carbonyl compounds, *e.g.* acetone, glyoxal, and formaldehyde, and subsequent heterogeneous chemistry, including oligomerization, dehydration, and aldol condensation, have been previously observed.[31–34,38,40] In previous studies with metal oxide surfaces,[31,32] the adsorption, chemistry and photochemistry of small carbonyl compounds have been investigated to understand heterogeneous chemistry. In the current study, we extend this aspect further to identify the products formed on these surfaces and investigate the detailed mechanism *via* isotope labeling experiments. Moreover, different from previous studies, the current effort focuses on the heterogeneous and multiphase chemistry of small carbonyl compounds on metal oxide surfaces, instead of salts such as ammonium sulfate aerosol particles.[33,34] In the presence of NO_x in the gas phase, MEK can lead to peroxyacetyl nitrate and ozone formation.[41,42] However, MEK reactions with trace gases such as NO_2 on mineral aerosol surfaces remain unknown.

In this study, the surface adsorption and surface reactions of MEK on mineral oxide surfaces, SiO_2, α-Fe_2O_3, and TiO_2 were investigated. SiO_2 is a major component in mineral dust, yet relatively inert, whereas α-Fe_2O_3 and TiO_2 are more reactive components.[43] MEK can adsorb onto and undergo heterogeneous reactions on these mineral surfaces. Furthermore, given the importance of water vapor in atmospheric reactions,[44] MEK adsorption on mineral surfaces under both dry and high relative humidity (RH) conditions was considered as well as the reactions of adsorbed-MEK with NO_2. NO_2 is found in the atmosphere, primarily emitted *via* fossil fuel combustion and vehicle exhausts,[45,46] and due to the higher correlation of atmospheric NO_2 concentrations to traffic, it is used as a traffic-related air pollution marker.[46] Therefore, interactions between MEK with mineral dust and NO_2 during dust transport and urban dust episodes can facilitate the formation of a range of oxygenated SOAs as discussed in detail here.

Most interesting, and discussed in more detail below, despite suggestions that small carbonyl compounds are too volatile to be significantly involved in heterogeneous chemistry

leading to SOA formation, is that this study provides insights into the formation of a range of SOAs from MEK on mineral surfaces that can occur. Both Fourier transform infrared (FTIR) spectroscopy as an *in situ* probe of product formation and high-resolution mass spectrometry (HRMS) of solvent-extracted products were used to unravel the complex heterogeneous chemistry occurring on mineral dust surfaces.

2 Materials and methods

2.1 Transmission FTIR spectroscopy and methods

Transmission FTIR spectroscopy was used to monitor reactions on oxide surfaces at 296 ± 1 K. Additional details of the infrared cell and gas handling system have been previously described.[47–52] Oxide particles (SiO_2, Aerosil OX50, α-Fe_2O_3, hematite, 99+%, Fischer Scientific, and TiO_2, rutile, Sigma Aldrich) with a BET surface area of $30 + 1$ m^2 g^{-1}, $80 + 10$ m^2 g^{-1}, and $31 + 4$ m^2 g^{-1}, respectively, were heated in an oven at 473 ± 1 K overnight to remove organic contaminants and then pressed onto one half of a tungsten grid (*ca.* 5 mg). The grid was then placed in the sample IR cell compartment, held by two stainless steel jaws. Following the preparation of the mineral sample and placement in the IR cell, the system was evacuated for 4 h using a turbomolecular pump. SiO_2 was further heated once pressed to the tungsten grid. α-Fe_2O_3 and TiO_2 surfaces were subsequently exposed to 50% RH water vapor for 2 h to ensure a fully hydroxylated terminated surface. Once hydroxylated, the system was evacuated for another 6 h to remove water vapor in the chamber. SiO_2 surfaces were not subjected to hydroxylation, as the surfaces have strong signals arising from silanol groups. The MEK adsorption mechanisms on α-Fe_2O_3 and TiO_2 surfaces were explored using deuterated water vapor in the surface hydroxylation step above. In particular, 10–20 Torr of D_2O (Sigma Aldrich, 99.9%) degassed *via* several cycles of the freeze–thaw–pump method was introduced into the IR cell loaded with either an α-Fe_2O_3 or TiO_2 surface for 30 min followed by evacuation. The process was repeated until the surface is fully deuteroxylated.[53,54]

After evacuation, the surface was exposed to the desired pressure of methyl ethyl ketone (MEK, 2-butanone, 99%, Sigma Aldrich) for 20 min under dry conditions (RH < 1%). The MEK sample was degassed at least three times with consecutive freeze–pump–thaw cycles prior to use. Then, in order to understand the impact of RH% on the adsorption of MEK on mineral surfaces, in a different set of experiments, 20 mTorr of MEK was introduced into the IR cell and allowed adsorption for 30 min. Then, the RH% inside the IR cell was brought to 80% by introducing water vapor and the reactions were monitored over 4 h. Following the adsorption, the surfaces were evacuated overnight. Similarly, the reactions of MEK with NO_2 on mineral surfaces were studied by introducing 5 mTorr of NO_2 (2 ppm in N_2, Airgas) into the IR cell after allowing 20 mTorr of MEK adsorption on mineral surfaces. Here, the reactions were monitored over 4 h, and the surfaces were evacuated overnight following the adsorption. Relatively higher concentrations of reactants compared to their atmospheric concentrations were used in this study to determine the feasibility of these types of reactions. Additionally, mass spectrometric analysis of surface

products required these higher concentrations for definitive confirmation.

Prior to and following the exposure to gases, single-beam spectra (250 scans) of the surface and gas phase were acquired using a resolution of 4 cm^{-1} and covering the spectral range of 600 to 4000 cm^{-1}. This was accomplished by the use of a linear translator with the infrared beam interrogating the portion of the grid pressed with mineral particles followed by the portion of the grid left blank. Absorption spectra on mineral particles are reported as the difference in the mineral spectra before and after exposure to gases. Absorption bands due to gas-phase components, as measured through the blank half of the tungsten grid under identical conditions, were subtracted to obtain the FTIR spectra of adsorbed species only.

2.2 High-resolution mass spectrometry

Organic products formed on mineral surfaces following the adsorption of MEK, and subsequent reactions with NO$_2$, were analyzed using a direct-injection linear ion trap (Thermo Fisher Orbitrap) high-resolution mass spectrometer (HRMS). Additional experiments with ~5 mg of two authentic dust samples, Arizona Test Dust (AZTD, Powder Technologies) and Gobi Dust (NIES, Japan),[55] were conducted by exposing them to 20 mTorr MEK for 30 min followed by evacuation. Adsorbed products were extracted from the solid substrate using methanol (CH$_3$OH, Fisher Scientific, HPLC grade) as the solvent. Methanol was chosen as the solvent as it produced the best signal for MEK standards. The sample vial, syringe, and all other glassware used in the transfer process were cleaned prior to use with methanol, and Milli-Q water (Millipore Sigma, 18.2 MΩ), and baked in an oven at 773 ± 1 K to further remove trace organics. Plastic vials used in sample preparation were sonicated in methanol for 60 min and washed thoroughly prior to use. All of the samples were stored at 253 ± 1 K and analyzed within 48 h of collection. Product stability was tested for up to 40 days under the freeze storage conditions used. It was determined that no transformations of products occurred.

HRMS analysis in both positive electrospray ionization (ESI) ([M + H]$^+$ and [M + Na]$^+$) and negative ESI modes ([M − H]) was used; however, structure elucidation was conducted with positive ESI mode data. The heated electrospray ionization (HESI) source was operated at 373.15 K. The ESI capillary was set to a voltage of 3.5 kV at 623.15 K. The HESI-Orbitrap MS was calibrated prior to use. Mass spectra were acquired with a mass range of 50–2000 Da. Peaks with a mass tolerance of > 5 ppm were rejected. Unconfirmed minor products (low intensity) are not reported. Compositions were calculated with the following element ranges: 12C, 0–60; 1H, 0–150; 2H, 0–50; 16O, 0–25; 14N, 0–3; 23Na, 0–5; 39K, 0–5; 56Fe, 0–5; 28Si, 0–5; 48Ti, 0–5. Tandem mass spectrometry (MS/MS) with a collision energy of 40 eV was used for structure determination.

3 Results and discussion

3.1 MEK adsorption and oligomerization on oxide surfaces

SiO$_2$ surfaces exposed to gas-phase MEK at various pressures under dry conditions show new spectral features due to surface
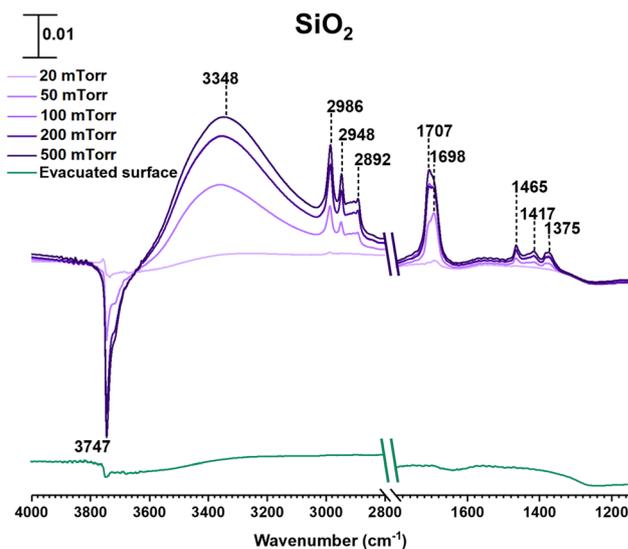

Fig. 1 FTIR spectra of MEK adsorption on the SiO$_2$ surface under dry conditions in the spectral regions from 1150 to 1800 cm^{-1} and 2800 to 4000 cm^{-1}. The absorbance scale is shown in the top left corner.

adsorption as seen in Fig. 1. Most notable are the infrared absorption bands in the regions extending from 2800 to 4000 cm^{-1} and 1150 to 1800 cm^{-1}. The bands between 2800 and 3000 cm^{-1} were assigned to C–H stretching vibrations and those between 1300 and 1500 cm^{-1} were assigned to C–H bending modes (Table 1).[56] The adsorbed carbonyl group on SiO$_2$ surfaces is observed at 1698 cm^{-1} and 1707 cm^{-1} indicating multilayer adsorption. Moreover, the carbonyl group of MEK interacts with silanol groups *via* H-bond formation. At relatively lower MEK pressures, the peak at 1698 cm^{-1} is stronger, whereas, at higher MEK pressures, the peak at 1707 cm^{-1} supersedes as adsorbed layers farther away from the surface have more gas-phase-like characteristics. These frequencies observed for the absorption bands found for adsorbed MEK correspond fairly closely to its gas-phase vibrational frequencies indicating that MEK is molecularly adsorbed onto SiO$_2$ surfaces.[57] The Gas-Phase-MEK FTIR spectrum is provided in ESI Fig. S1.†

A loss at 3747 cm^{-1} suggests that isolated silanol groups on the silica surface are interacting *via* hydrogen bonding with MEK molecules.[58,59] Furthermore, a band for the hydrogen bond between MEK and the silanol group appears with an absorption maximum at 3348 cm^{-1}. Upon evacuating overnight, almost all of the adsorbed MEK is removed, thus suggesting reversible adsorption of MEK on SiO$_2$ surfaces. Additionally, HRMS analysis of samples extracted from MEK-treated surfaces while outside the acceptable mass tolerance limits detected only a minor quantity of residual MEK (C$_4$H$_8$ONa, m/z 95.05) in positive ESI mode. No MEK derivatives were confirmed during the HRMS analysis. This indicates that adsorbed MEK does not transform into other compounds on SiO$_2$ under dark and dry conditions. The HRMS pattern for the MEK standard in methanol is provided in Fig. S2.† Briefly, at lower MEK standard concentrations (70 ppm), the sodated MEK monomer was

© 2023 The Author(s). Published by the Royal Society of Chemistry

Environ. Sci.: Atmos., 2023, **3**, 799–815 | **801**

Table 1 FTIR peak assignments in the frequency range from 1200 to 3000 cm^{-1} of adsorbed MEK on oxide surfaces[31,32,56,58,61]

Vibrational mode	Peak assignment		
	SiO_2	$\alpha\text{-}Fe_2O_3$	TiO_2
Loss of isolated silanol groups	3747	—	—
Loss of surface hydroxyl groups	—	3670, 3620	—
Hydrogen bond network formation	3348	—	—
C–H bond stretching vibrations	2986, 2948, 2892	2971, 2941, 2910, 2883, 2855	2970, 2939, 2888
C=O bond stretching	1698,1701	1683	1690
Adsorbed water, bending vibration	—	1635	1648
C=C bond stretching of an alpha-beta unsaturated ketone, and other conjugated systems	—	1615, 1568	1580
C–H bond bending vibrations	1465, 1417, 1375	1464, 1410, 1381, 1367, 1340	1461, 1408, 1390, 1364
C–O bond stretching vibrations, particularly of alcohols	—	1281, 1242, 1202, 1175	1264, 1184

observed at $m/z = 95.05$ for C_4H_8Ona, whereas, at higher MEK concentrations (1000 ppm), a sodated MEK 'dimer' was identified at $m/z = 167.10$. MS/MS fragmentation of this peak produced one major fragment at 95.05 suggesting cluster formation during chemical ionization (Table S1†).[60] However, no other MEK clusters/'oligomers' were observed in the 1000 ppm MEK standard during HRMS analysis (Fig. S2†).

In contrast to SiO_2 surfaces, MEK-exposed $\alpha\text{-}Fe_2O_3$ surfaces show the appearance of additional spectral features suggesting the transformation of MEK to other adsorbed species on the surface (Fig. 2). These features include the shifting of the carbonyl peak to 1683 cm^{-1} along with the appearance of new peaks around 1615 and 1568 cm^{-1} (consistent with C=C stretching vibrations).[31,32,56,62] These spectral features indicate the formation of alpha-beta unsaturated ketones and conjugated compounds on the $\alpha\text{-}Fe_2O_3$ surface. Furthermore, peaks in the spectral region from 1150 to 1290 cm^{-1} for C–O bond vibrations indicate the formation of alcohol groups. Unlike on SiO_2 surfaces, it is important to note the formation of water as indicated by the presence of the adsorbed water bending vibration at ~1635 cm^{-1}.[51,56] MEK-exposed TiO_2 surfaces show similar spectral features. While a shoulder at ~1648 cm^{-1} appears suggesting the presence of adsorbed water, on TiO_2 surfaces, the feature is not as prominent as on $\alpha\text{-}Fe_2O_3$ surfaces. The adsorbed organic species were extracted in methanol and were further analyzed using HRMS for the identification and structure elucidation of the products formed. MS/MS was performed for identified compounds to confirm their structures. The full list of these fragmentation patterns is provided in Table S1†. Moreover, when assigning C=C bonds to these structures, particularly for dehydration products, overall theoretical stability due to extended conjugation and MS/MS fragmentation patterns were considered. The stereochemistry of molecules was not taken into account with these structural assignments.

Three groups of oligomers were identified on both $\alpha\text{-}Fe_2O_3$ and TiO_2 surfaces (Fig. 3 and Table 2). These oligomer groups are Group A: MEK dimer, Group B: MEK trimer and its derivatives (dehydration products), and Group C: MEK tetramer and its derivatives (dehydration products). For both $\alpha\text{-}Fe_2O_3$ and TiO_2 surfaces, a MEK dimer (Compound 1, $C_8H_{16}O_2Na$, $m/z =$ 167.10) was observed with the highest relative abundance. However, a dehydrated product of MEK dimer was not observed. This differs from acetone adsorption on TiO_2, in which mesityl oxide, a dehydration product of acetone aldol-condensation reaction, was observed.[32] MS/MS analysis of the m/z peak at 167.10 produced major fragments at $m/z = 95.05$ for C_4H_8ONa and 138.03 for $C_6H_{11}O_2Na$. Another fragment was identified at $m/z = 127.11$ for $C_8H_{15}O$, for water loss during MS/MS analysis, which supports the presence of an OH group that is eliminated as water. The MS/MS fragmentation pattern of $m/z = 167.10$ for solvent-extracted samples is particularly different from that of high-concentration MEK standard samples (1000 ppm) where one fragment at $m/z = 95.05$ for the MEK monomer was observed (Fig. S2† and Table S1†). This indicates that at higher concentrations, the standard sample produced a 'dimer' under MS conditions, commonly known as cluster formation,[60] while on surfaces, a dimer is formed from surface reactions with the structure of compound 1.

Additionally, a MEK trimer (Compound 2, $C_{12}H_{24}O_3Na$, $m/z = 239.16$) and two dehydration products (Compound 3, $C_{12}H_{22}O_2Na$, $m/z = 221.15$ and Compound 4, $C_{12}H_{20}ONa$, $m/z = 203.14$) were identified on both $\alpha\text{-}Fe_2O_3$ and TiO_2 surfaces, along with their fragments. The MS/MS analysis of the peak at $m/z = 239.10$ produced a fragment at 221.15 for $C_{12}H_{22}O_2Na$, whereas the fragmentation of the peak at $m/z = 221.15$ produced several different fragments notably at $m/z = 95.05$ (MEK monomer unit), 203.14 ($C_{12}H_{20}ONa$) and, 151.07 ($C_7H_{12}O_2Na$). The evidence of forming a MEK tetramer and its dehydration products was observed on both $\alpha\text{-}Fe_2O_3$ and TiO_2 surfaces. On $\alpha\text{-}Fe_2O_3$ surfaces, four different compounds, namely, MEK tetramer (Compound 5, $C_{16}H_{32}O_4Na$, $m/z = 311.22$), Compound 6 ($C_{16}H_{30}O_3Na$, $m/z = 293.20$), Compound 7 ($C_{16}H_{28}O_2Na$, $m/z = 275.20$), and Compound 8 ($C_{16}H_{26}ONa$, $m/z = 257.19$), were observed with a higher relative abundance than group B compounds. However, on TiO_2 surfaces, only Compounds 7 and 8 were observed with a lower relative abundance than group B compounds. This indicates that the tetramer formation is favored on $\alpha\text{-}Fe_2O_3$ surfaces over TiO_2 underscoring the role of specific mineral surfaces in the oligomerization of MEK. Such carbonyl compound oligomerization
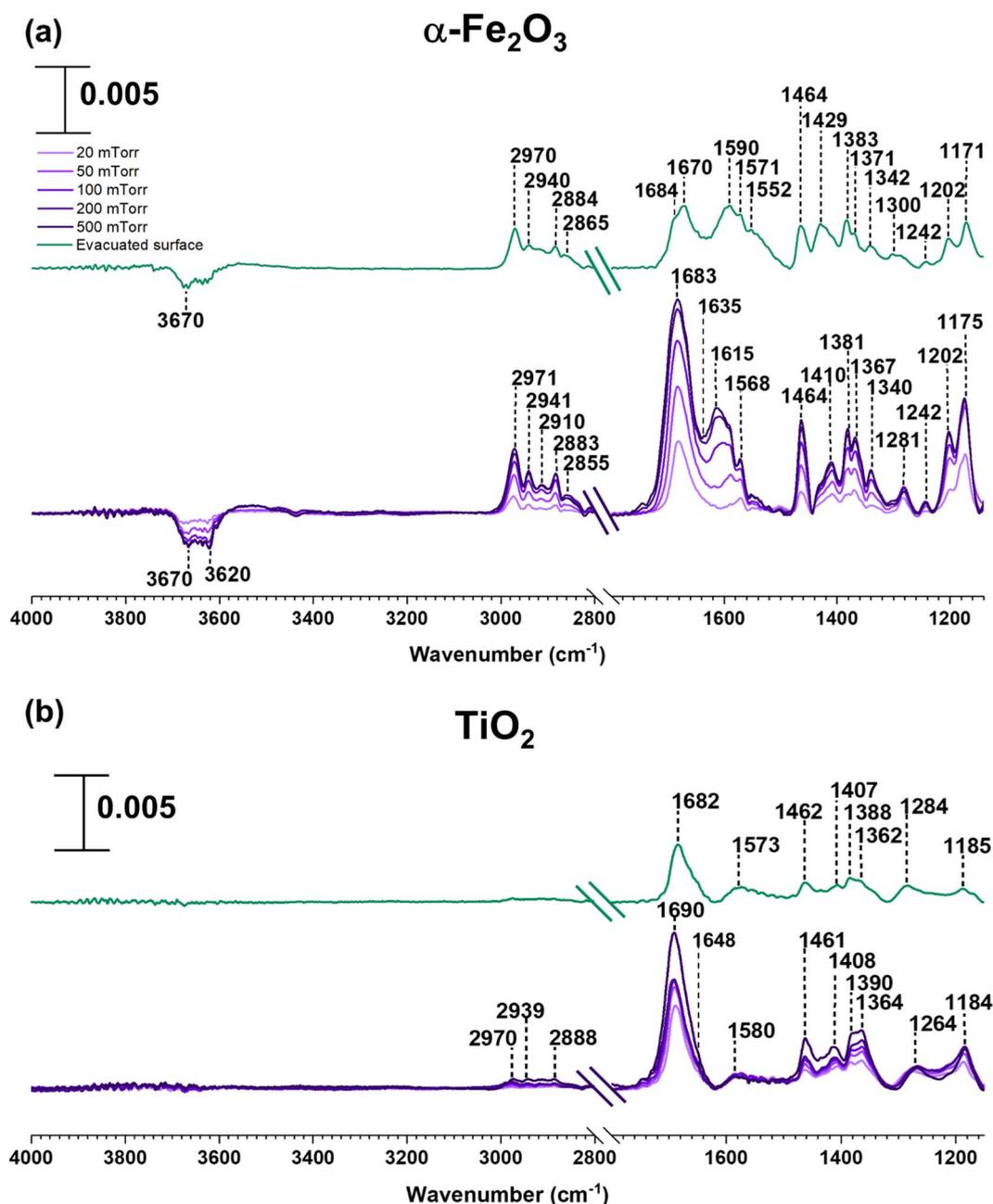
Fig. 2 FTIR spectra of MEK adsorption on (a) α-Fe$_2$O$_3$ and (b) TiO$_2$ under dry conditions in the spectral regions from 1150 to 1800 cm^{-1} and 2800 to 4000 cm^{-1}. The absorbance scale is shown in the top left corner.

has previously been observed with pinonaldehyde on acidic aerosols such as mixtures of (NH$_4$)$_2$SO$_4$ and H$_2$SO$_4$.[63] Furthermore, these HRMS data are complemented by the FTIR spectra produced by the adsorption of MEK on these oxide surfaces, in which the spectral features show the formation of conjugated carbonyl systems and alcohol groups. Furthermore, HRMS analysis of surface products with varying MEK initial pressures in the range used in this study shows no change in oligomer distribution. Additionally, adsorbed water observed in part is due to the dehydration of MEK oligomers formed on surfaces.

Numerous laboratory and field observations indicate the formation of various oligomers of smaller atmospheric carbonyls and their derivatives. However, most of these studies are limited to photochemical and/or aqueous phase conditions,[40,64–66] while a limited understanding exists for small carbonyl-oligomerization in multiphase chemistry.[12,31,32,38] Thus, our study provides new evidence on mineral-specific heterogeneous reactions of MEK.

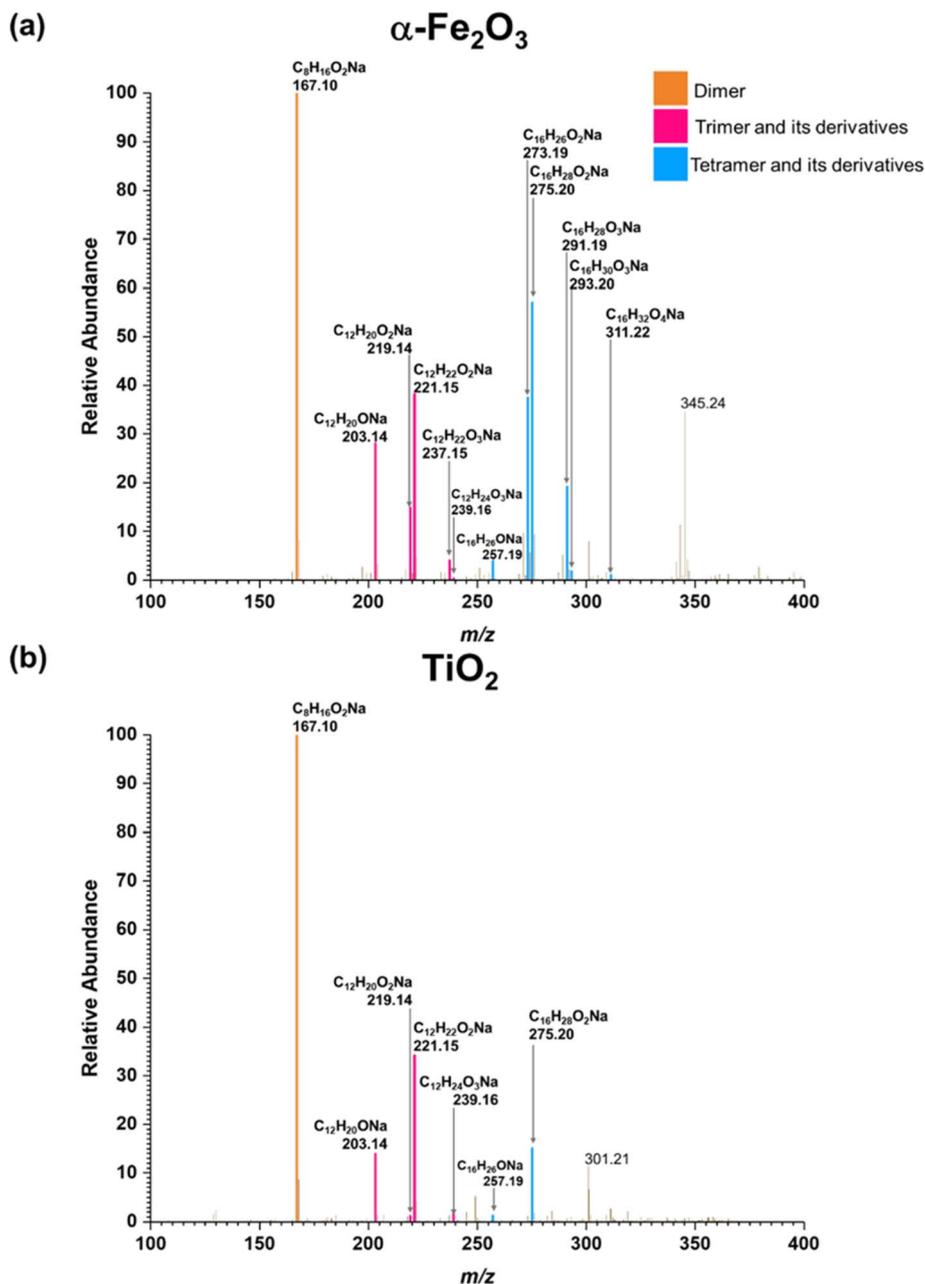The formation of a series of oligomers on α-Fe$_2$O$_3$ and TiO$_2$ surfaces can be explained by surface-mediated keto–enol

© 2023 The Author(s). Published by the Royal Society of Chemistry

Environ. Sci.: Atmos., 2023, **3**, 799–815 | **803**

Fig. 3 HRMS patterns of surface products formed upon adsorption of MEK on (a) α-Fe_2O_3 and (b) TiO_2 under dry conditions.
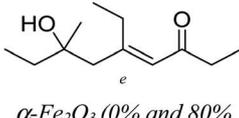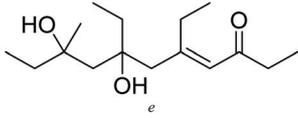
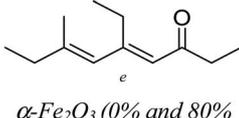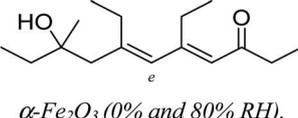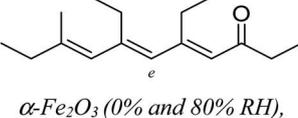tautomerism (KET) followed by aldol condensation of MEK[67] (Schemes 1 and 2). The oligomerization can occur *via* two reaction pathways. Both α-Fe_2O_3 and TiO_2 surfaces are known to contain surface hydroxyl groups. MEK may strongly adsorb onto Lewis acid sites (Fe^{3+} or Ti^{4+}) and reduced defect sites (Fe^{2+} or Ti^{3+}) on oxide surfaces followed by the formation of a surface–enolate complex.[31,32,61,68] This is followed by abstraction of a proton from MEK (α-H) by either surface oxygen atoms or surface hydroxyl groups. The interaction of MEK with surface O–H groups is suggested by the FTIR data as a loss of surface O–H groups (3620 and 3670 cm^{-1}) from α-Fe_2O_3 is seen. A similar aldol-condensation mechanism has previously been proposed with acetone by other investigators on oxide surfaces

with acidic or basic properties such as TiO_2, α-Fe_2O_3, and α-Al_2O_3.[31,32,62]

The MEK dimer and oligomer formation mechanisms on mineral oxide surfaces were explored using fully deuteroxylated α-Fe_2O_3 and TiO_2 surfaces. Surface deuteroxylation was conducted by exposing surfaces to ~10 Torr of D_2O repeatedly until complete surface deuteroxylation is achieved.[53,54] Then, 100 mTorr of MEK was exposed to the deuteroxylated α-Fe_2O_3 or TiO_2 surface for over 4 h followed by overnight evacuation (Fig. S3† and Table S2†). Upon exposure to MEK, loss of O-D groups on α-Fe_2O_3 surfaces is seen around 2708 and 2672 cm^{-1} due to their interaction with MEK whereas new spectral features appeared around 2600 cm^{-1} suggesting the

Paper

Table 2   Identified surface products formed from MEK oligomerization on oxide surfaces

| Group A – MEK dimer		Group B – MEK trimer and its derivatives		Group C – MEK tetramer and its derivatives	
Compound 1 167.10 [a] $C_8H_{16}O_2Na$ [b] $(C_8H_{16}O_2)$ [c] $\alpha\text{-}Fe_2O_3$ (0% and 80% RH), TiO_2 (0% and 80% RH) [d]		**Compound 2** 239.16 $C_{12}H_{24}O_3Na$ $(C_{12}H_{24}O_3)$ $\alpha\text{-}Fe_2O_3$ (0% and 80% RH), TiO_2 (0% and 80% RH)		**Compound 5** 311.22 $C_{16}H_{32}O_4Na$ $(C_{16}H_{32}O_4)$ [e] $\alpha\text{-}Fe_2O_3$ (0% and 80% RH), TiO_2 (80% RH)	
		Compound 3 221.15 $C_{12}H_{22}O_2Na$ $(C_{12}H_{22}O_2)$ [e] $\alpha\text{-}Fe_2O_3$ (0% and 80% RH), TiO_2 (0% and 80% RH)		**Compound 6** 293.20 $C_{16}H_{30}O_3Na$ $(C_{16}H_{30}O_3)$ [e] $\alpha\text{-}Fe_2O_3$ (0% and 80% RH), TiO_2 (80% RH)	
		Compound 4 203.14 $C_{12}H_{20}ONa$ $(C_{12}H_{20}O)$ [e] $\alpha\text{-}Fe_2O_3$ (0% and 80% RH), TiO_2 (0% and 80% RH)		**Compound 7** 275.20 $C_{16}H_{28}O_2Na$ $(C_{16}H_{28}O_2)$ [e] $\alpha\text{-}Fe_2O_3$ (0% and 80% RH), TiO_2 (0% and 80% RH)	
				Compound 8 257.19 $C_{16}H_{26}ONa$ $(C_{16}H_{26}O)$ [e] $\alpha\text{-}Fe_2O_3$ (0% and 80% RH), TiO_2 (0% and 80% RH)	
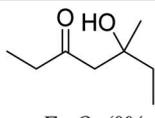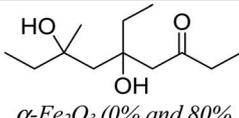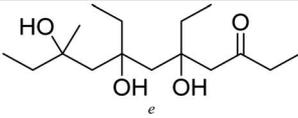
[a]: m/z. [b]: Observed formula. [c]: Molecular formula. [d]: Mineral oxide surface and relative humidity (%RH) of the compounds observed. [e]: C=C was assigned based on the most stable structure due to the formation of conjugated systems and/or MS/MS fragmentation patterns.

formation of an OD, H-bond network. Furthermore, spectral features corresponding to C–D bond formation were observed from 2119–2500 cm^{-1}. Additionally, a smaller peak around 3620 cm^{-1} begun to appear along with the evidence of OH and H-bond formation at ~3458 cm^{-1}. FTIR spectra indicate that surface originated deuterium atoms get incorporated with surface products formed while MEK originated H atoms get incorporated with the surface, forming surface hydroxyl groups. For deuteroxylated TiO_2 spectra, some spectral features corresponding to the loss of surface O-D groups were seen whereas no significant changes were observed around ~3600 cm^{-1} corresponding to surface O–H groups. Adsorbed species extracted to methanol was analyzed via HRMS for deuterated products of MEK dimer and oligomers (Fig. S4† and Table S3†).

As shown in Scheme 1a & b on mineral surfaces, surface hydroxyl/deuteroxyl groups were protonated by a methyl hydrogen from MEK, thereby producing surface-adsorbed water molecules. Thus, this mechanistic pathway suggests another source of surface-adsorbed water seen in the FTIR spectra (bending mode of water at 1635 cm^{-1} on $\alpha\text{-}Fe_2O_3$ and 1648 cm^{-1} on TiO_2). In isotope labeling experiments, deuterated products of MEK dimer and oligomers were observed in HRMS analysis for both surfaces, confirming the exchange of surface

hydrogens from hydroxyl groups to the products formed on surfaces (Fig. S4 and S5†). Furthermore, for $\alpha\text{-}Fe_2O_3$ surfaces, during enolate formation, most α-H of MEK is exchanged with deuterium atoms from surface deuteroxyl groups indicating the constant proton-exchange nature between the enolate and the surface. This is further complimented by the appearance of FTIR spectral features for surface OH groups on deuterated $\alpha\text{-}Fe_2O_3$ surfaces upon exposure to MEK (Fig. S3†). For TiO_2 surfaces, while deuterated oligomers were observed, the products with higher deuteration were observed with a lower intensity. For example, for $\alpha\text{-}Fe_2O_3$ surfaces, $C_8H_9D_7O_2$ was observed with the highest intensity for the deuterated MEK dimer group (Fig. S4†), whereas for TiO_2 surfaces, $C_8H_{11}D_5O_2$ was observed with the highest intensity for the same group. This trend with a higher degree of deuteration was seen among the other oligomer groups observed on $\alpha\text{-}Fe_2O_3$ surfaces compared to that of TiO_2 surfaces (Table S3†). This higher degree of deuteration may correspond to higher surface hydroxyl group density on $\alpha\text{-}Fe_2O_3$ surfaces than TiO_2 as observed in FTIR spectra. For the deuterated MEK dimer, for both $\alpha\text{-}Fe_2O_3$ and TiO_2 surfaces, no more than 9 deuterium atoms were observed suggesting that the deuteration of the MEK molecule can occur prior to dimerization (Scheme 1a, Fig. S4, S5 and Table S3†).
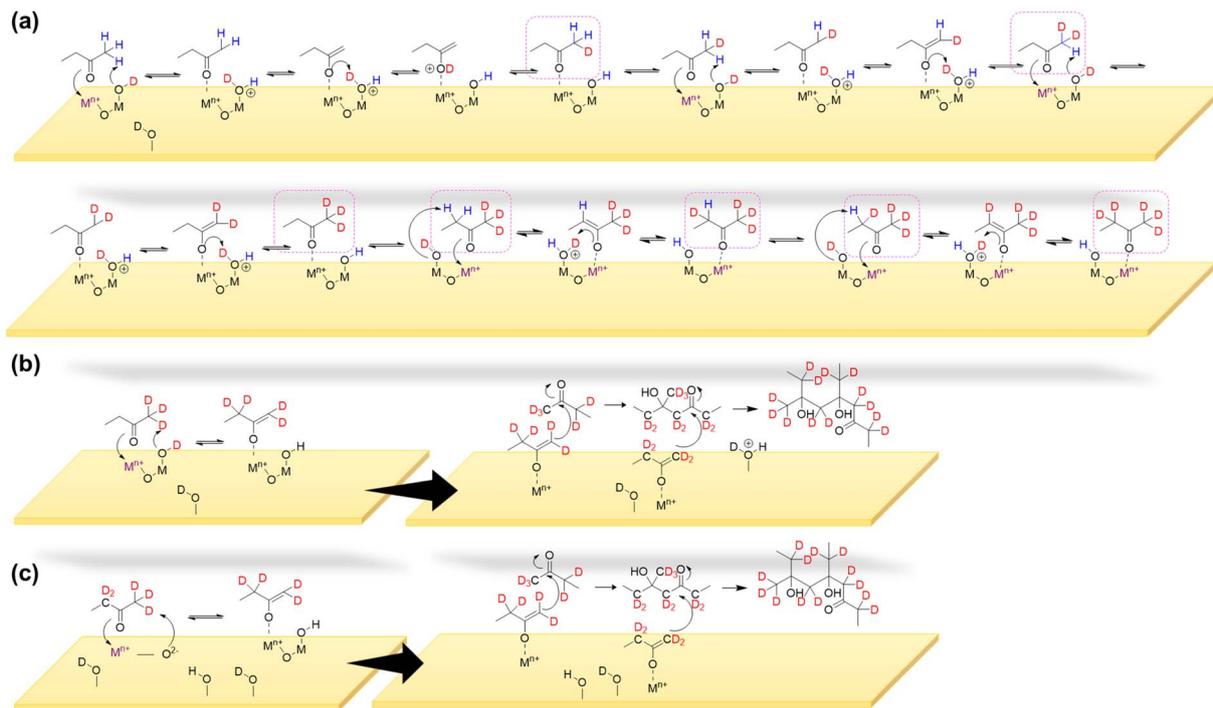
Scheme 1 (a) Deuteration of α-H on the MEK molecule upon exposure to the deuteroxylated surface. Formation of a surface-adsorbed MEK enolate complex *via* keto–enol tautomerism (KET) on mineral oxide surfaces due to MEK strongly adsorbing onto Lewis acid sites (Fe^{3+} and Ti^{4+}) and hydrogen abstraction (b) by surface hydroxyl/deuteroxyl groups, and (c) by surface O^{2-} sites. The surface-adsorbed MEK-enolate-complex undergoes dimerization and oligomerization *via* self- and cross-condensation respectively. Deuterated MEK oligomers with maximum possible deuteration are shown to reflect proton migration.
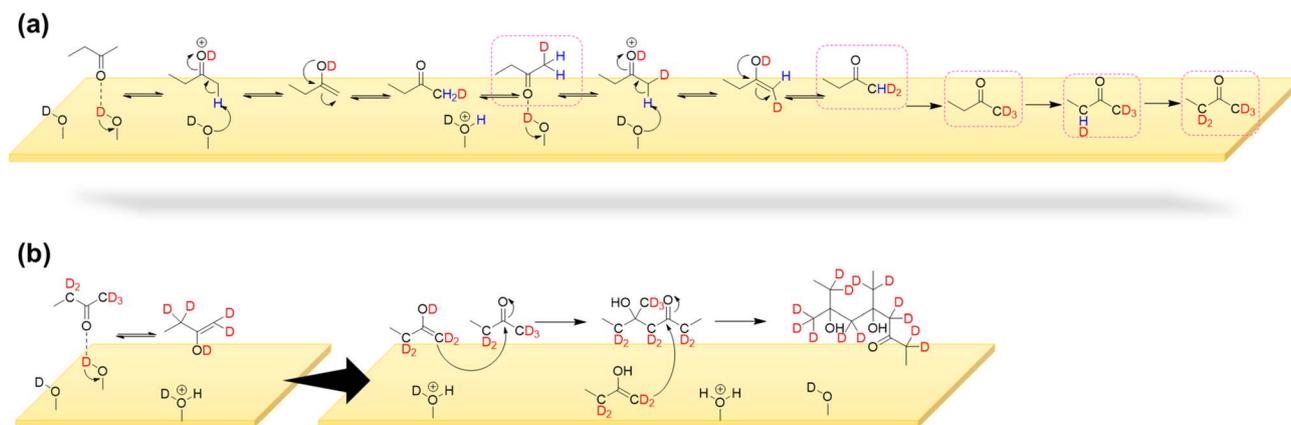
Scheme 2 (a) Deuteration of MEK molecules and (b) formation of MEK enol *via* keto–enol tautomerism (KET) on mineral oxide surfaces as a result of the interaction of MEK with surface hydroxyl/deuteroxyl groups *via* H-bond formation, followed by dimerization and oligomerization *via* self- and cross-condensation respectively. Deuterated MEK oligomers with maximum possible deuteration are shown to reflect the proton migration.

Once the surface-adsorbed MEK-enolate-complex is formed, it self-condensates with another MEK molecule to form a MEK dimer, or cross-condensates with another MEK dimer (or oligomer) to form either a MEK trimer or a tetramer.

A surface-adsorbed enolate complex forms *via* H abstraction by surface oxygen sites resulting in a similar aldol-condensation pathway (Scheme 1c)[61] which makes this reaction pathway also possible. The highest relative abundance of MEK dimer

observed suggests that the formation of trimers and tetramers may be challenging due to the surface-adsorbed nature of the enolate complex. In these schemes, the abstraction of a methyl H is considered, although the abstraction of α-H from the ethyl group of MEK may form a more stable enolate form owing to substitution. The formation of the fragment $C_6H_{11}O_2Na$ from MEK dimer ($m/z = 167.10$) suggests that **1** is an ethyl ketone (its enolate formed by the abstraction of methyl H), instead of a methyl ketone.

In another formation pathway, the surface hydroxyl groups and adsorbed water induce the formation of MEK enol which then undergoes self-condensation with another MEK molecule to form a MEK dimer (Scheme 2). Hydrogen exchange from surface hydroxyl groups to MEK molecules can also be expected during this mechanistic pathway, deuterating α-H atoms. Further formation of MEK enol may continue to cross-condensate, forming other MEK oligomers. The MEK enol formation occurs near the surface as opposed to the adsorbed enolate complex explained in Scheme 1, making it less challenging to form oligomers with 3 or 4 MEK units. Surface-adsorbed water on α-Fe₂O₃ surfaces appears to enhance the KET of protonated MEK, facilitating a higher relative abundance of MEK trimer and tetramer in comparison to their relative abundances on TiO₂ surfaces, once again highlighting the important role the mineral surface plays (Fig. 3). Here, the relative abundance was considered with respect to the 100% relative abundance of the particular HRMS scan. The role of water molecules in the oligomerization of MEK on mineral surfaces is discussed in detail in below.

Additionally, studies conducted with the two authentic dust samples, Arizona Test Dust (AZTD) and Gobi Dust, showed the formation of similar oligomers from MEK on these surfaces. For AZTD, all Compounds **1–8** was identified (Fig. S6†). However, for Gobi dust, the formation of MEK dimer mostly was observed.

3.2 Surface product formation from adsorbed MEK in the presence of high relative humidity

As discussed above, water can play an important role in the reaction chemistry of MEK on oxide surfaces. In order to further investigate the role of water molecules in MEK oligomerization, experiments were conducted at 80% RH. Fig. 4 shows the infrared spectrum of surfaces following exposure to MEK and water vapor after 4 h. On SiO₂, upon exposure to water vapor, an adsorbed water bending vibration appears at 1628 cm⁻¹ and a broad hydrogen stretching region is observed from 3380 to 3300 cm⁻¹. Upon evacuation of the infrared cell, almost all adsorbed species were desorbed into the gas phase leaving little signal observed. However, at 80% RH, MEK-adsorbed α-Fe₂O₃ surfaces started to develop additional spectral features, notable at 3700 cm⁻¹ (alcohol, free O–H stretching), at 3460, 3307, and 3543 cm⁻¹ for strong H-bonded networks of adsorbed water, MEK, and alcohols, and at 1635 cm⁻¹ (adsorbed water bending vibration). Furthermore, once evacuated, the surface retained most of these spectral features, although with a lower intensity, and with fewer spectral features in the region from 1150 to
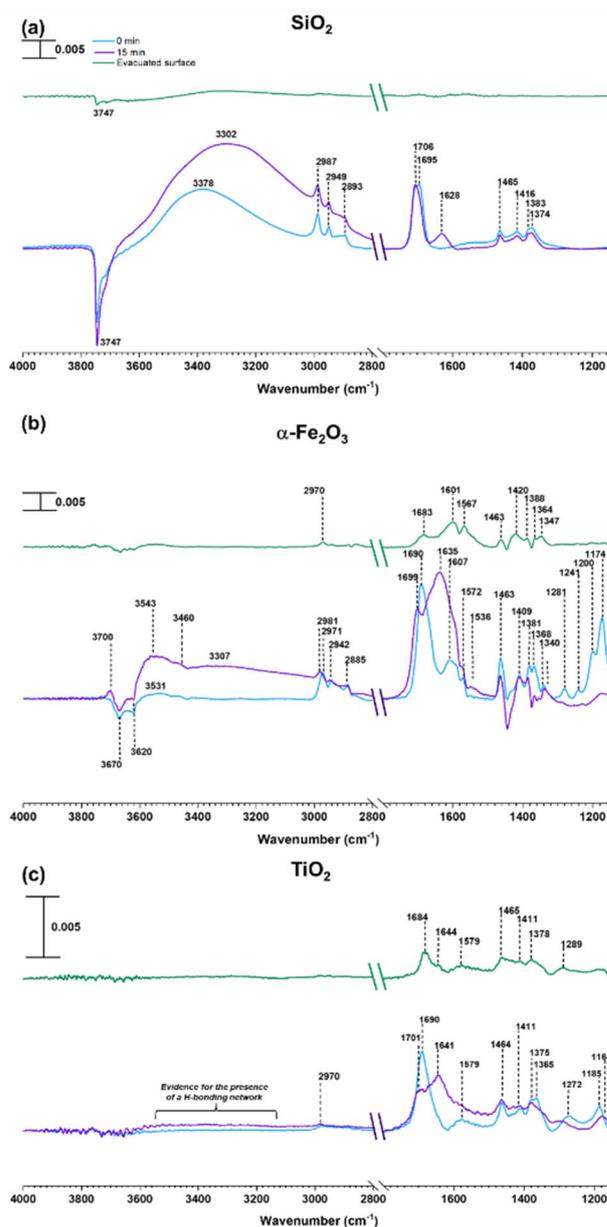

Fig. 4 FTIR spectra of MEK adsorption at 80% relative humidity (RH) on (a) SiO₂, (b) α-Fe₂O₃, and (c) TiO₂ in the spectral regions from 1150 to 1800 cm⁻¹ and 2800 to 4000 cm⁻¹. The absorbance scale is shown in the top left corner.

1690 cm⁻¹, indicating significant changes to the surface chemistry in the presence of adsorbed water. In contrast to α-Fe₂O₃ surfaces, evidence for an only weakly adsorbed H-bond network was observed on MEK-exposed TiO₂ surfaces at 80% RH. However, adsorbed water on the surface was observed at 1641 cm⁻¹ (water bending vibration) along with the presence of adsorbed-MEK spectral features comparable to those under dryer conditions. Upon evacuation, most of these spectral features were retained on the surface. The solvent-extracted products were further analyzed with HRMS and MS/MS to identify the product formation on each surface.
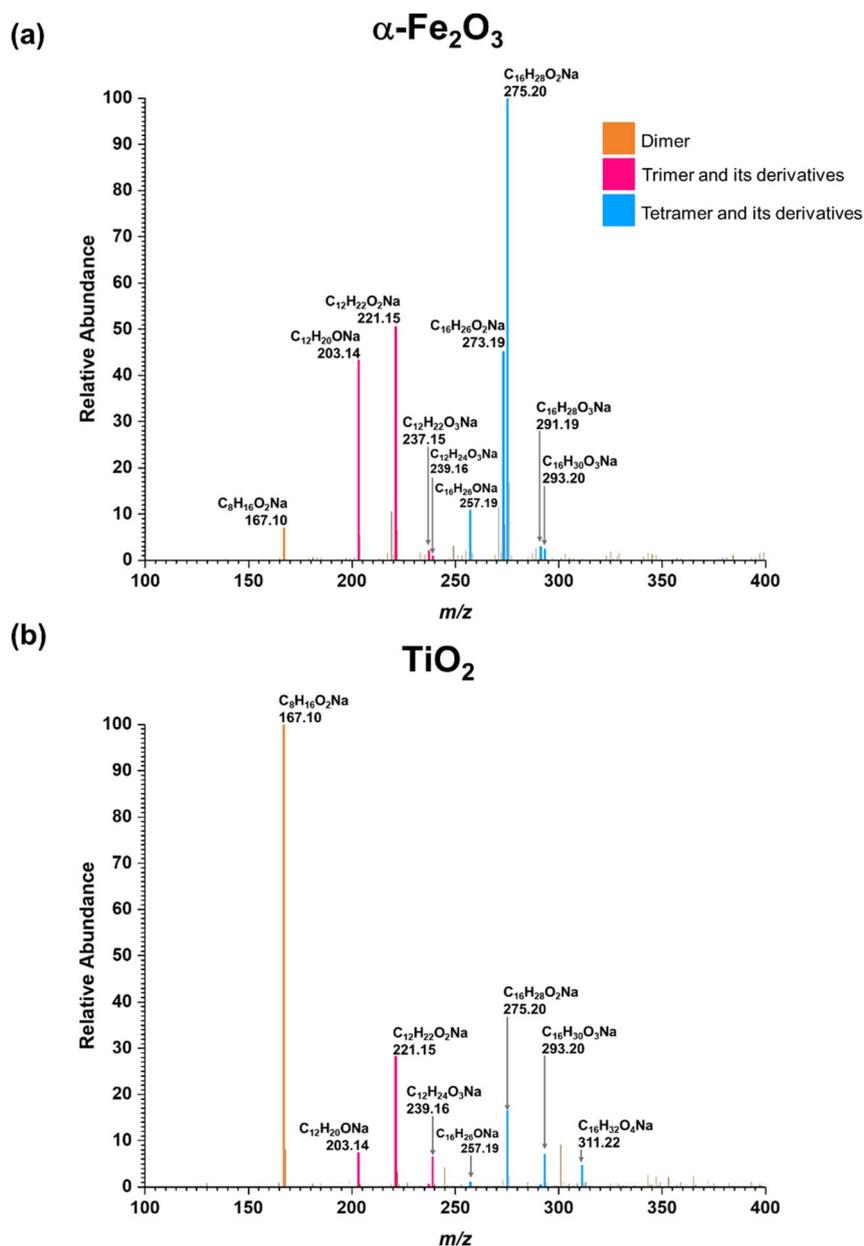
© 2023 The Author(s). Published by the Royal Society of Chemistry

Environ. Sci.: Atmos., 2023, **3**, 799–815 | **807**

Fig. 5 HRMS patterns of surface products formed upon adsorption of MEK at 80% RH on (a) α-Fe$_2$O$_3$ and (b) TiO$_2$.

All compounds (**1–8**) observed under the dry conditions were also observed under humid conditions on both α-Fe$_2$O$_3$ and TiO$_2$ surfaces (Fig. 5). However, the relative distribution of compounds significantly differed. For α-Fe$_2$O$_3$ surfaces, the relative abundance of MEK dimer ($m/z = 167.10$) decreased more than 10-fold under humid conditions while the dehydrated products of both MEK trimer ($m/z = 203.14$, 221.15) and MEK tetramer ($m/z = 257.19$, 275.20) increased by $\sim$1.5-fold, 1.3-fold, 3-fold, and 1.7-fold respectively suggesting the enhanced formation of MEK trimer and tetramer, and their dehydration products at higher RH. A qualitative analysis was not conducted for the corresponding peaks for MEK trimer and tetramer due to their lower relative abundances. For TiO$_2$, the

relative abundance of MEK dimer remained at 100% upon exposure to 80% RH. Nevertheless, the relative intensities of the HRMS peaks corresponding to MEK trimer ($m/z = 239.16$) and tetramer ($m/z = 311.22$, 293.20) were increased by $\sim$7-fold, $\sim$7-fold, and $\sim$18-fold respectively in comparison to their dryer counterparts indicating increased trimer and dimer formation on TiO$_2$ surfaces as well in the presence of water vapor.

Adsorbed water on both α-Fe$_2$O$_3$ and TiO$_2$ surfaces can introduce an additional oligomerization pathway *via* surface-induced enol formation as explained in Scheme 2. Water may also act as a catalyst for the KET step.[69,70] Higher relative humidity conditions such as those simulated in these experiments produce a strong H-bonded-water network with MEK
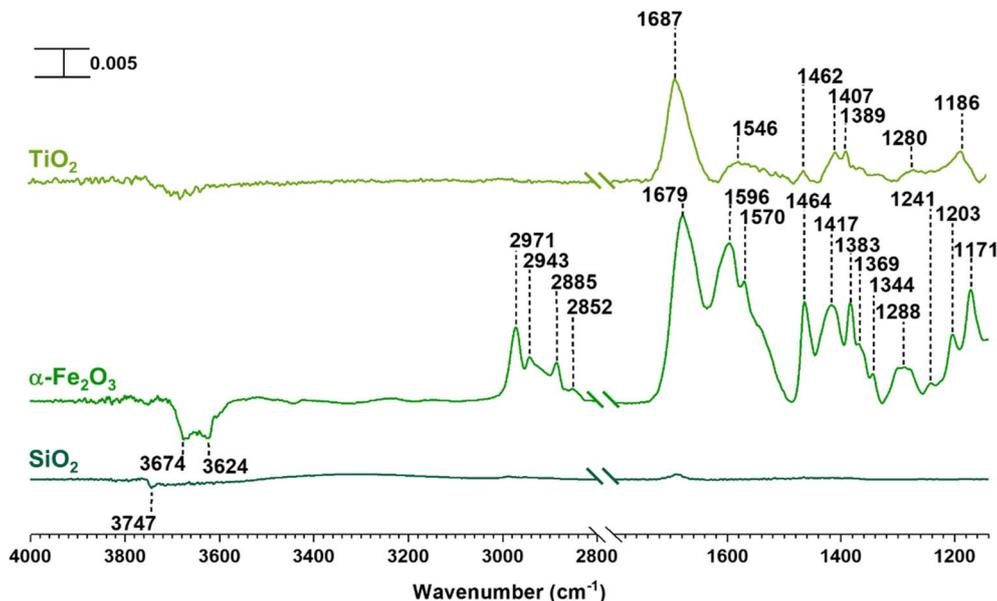
Fig. 6 FTIR spectra of evacuated surfaces of MEK reactions with NO_2 on SiO_2, α-Fe_2O_3, and TiO_2 under dry conditions in the spectral regions from 1150 to 1800 cm^{-1} and 2800 to 4000 cm^{-1}. The absorbance scale is shown in the top left corner.

molecules,[71] and on the surface as supported by the FTIR spectra of MEK-exposed α-Fe_2O_3 at 80% RH (Fig. S3†). The formation of these H-bonds induces KET as well as stabilizes the enol form of MEK.[71,72] Therefore, the observed increase of high-molecular-weight oligomers of MEK on α-Fe_2O_3 (predominantly) and TiO_2 surfaces at 80% RH may be due to the enhanced enolization on the surface. Furthermore, the better ability of α-Fe_2O_3 surfaces to form a strong H-bonded network than TiO_2 surfaces as observed in FTIR spectra and specifics of the H-bond networks such as bond strengths, lengths, and orientations[73,74] may have led to the formation of MEK trimer and tetramer with higher relative abundance on α-Fe_2O_3 than that of TiO_2 surfaces. Furthermore, given that SiO_2 is a neutral surface that only facilitates physisorption of both MEK and water molecules, the acidity of adsorbed water may be insufficient to induce KET.[75,76] Although, small carbonyls undergo hydration followed by polymerization in the atmosphere,[34,38] such a reaction was ruled out in these systems due to the absence of relevant HRMS evidence. The MEK surface coverages were determined from volumetric measurements[77] and for α-Fe_2O_3 and TiO_2 these were calculated to be 1.1×10^{14} and 9.3×10^{13} molecules per cm^2, respectively at an initial MEK pressure of 20 mTorr. Thus, these findings underscore the role of mineral oxide surfaces in not only the adsorption of atmospherically relevant ketones such as MEK but also in surface-mediated product formation under varying environmental conditions such as RH%.

3.3 Degradation followed by cross-condensation reaction of MEK with NO_2 on α-Fe_2O_3 surfaces

The reactions of MEK-adsorbed mineral surfaces with NO_2 (g) were studied under dry conditions. For all three surfaces, upon exposure to NO_2 (g), no visibly significant changes were observed on FTIR spectra. On evacuated SiO_2 surfaces, all but residual quantities of MEK were desorbed (Fig. 6). For evacuated α-Fe_2O_3 surfaces, spectral features in the C–H stretching vibration region remained the same in comparison to those of MEK only. However, slight differences in spectral features between 1670 and 1690 cm^{-1} were observed, perhaps indicating changes in the surface product speciation. No major differences were observed on the FTIR spectrum of evacuated TiO_2 surfaces, however, suggesting predominantly surface-mediated additional reaction pathways on α-Fe_2O_3 surfaces. Furthermore, no evidence was found for adsorbed organonitrates and/or adsorbed nitrate species formation on either surface. The solvent-extracted samples were analyzed with HRMS and MS/MS.

All compounds from **1–8** were identified on both MEK-adsorbed α-Fe_2O_3 and TiO_2 surfaces exposed to NO_2(g). Interestingly, **5** and **6** which were not present on MEK-exposed TiO_2 surfaces were identified when allowed reaction with NO_2, suggesting increased oligomerization in the presence of NO_2. Moreover, a range of new compounds were observed on α-Fe_2O_3 surfaces highlighting the surface-specific reactions involving MEK and NO_2 (Fig. 7 and Table 3). These compounds are acetaldehyde dimer (Compound **9**, $C_6H_{12}O_2Na$, $m/z = 139.07$), and its dehydration product (Compound **10**, $C_6H_{10}ONa$, $m/z = 121.05$), Compound **11** ($C_7H_{14}O_2Na$, $m/z = 153.09$), Compound **12** ($C_{14}H_{28}O_4Na$, $m/z = 283.19$), Compound **13** ($C_{14}H_{26}O_3Na$, $m/z = 265.18$), Compound **14** ($C_{14}H_{24}O_2Na$, $m/z = 247.17$), Compound **15** ($C_{14}H_{22}ONa$, $m/z = 229.16$), Compound **16** ($C_8H_{16}O_3Na$, $m/z = 183.10$), Compound **17** ($C_8H_{14}O_2Na$, $m/z = 165.09$), and Compound **18** ($C_8H_{12}ONa$, $m/z = 147.08$).
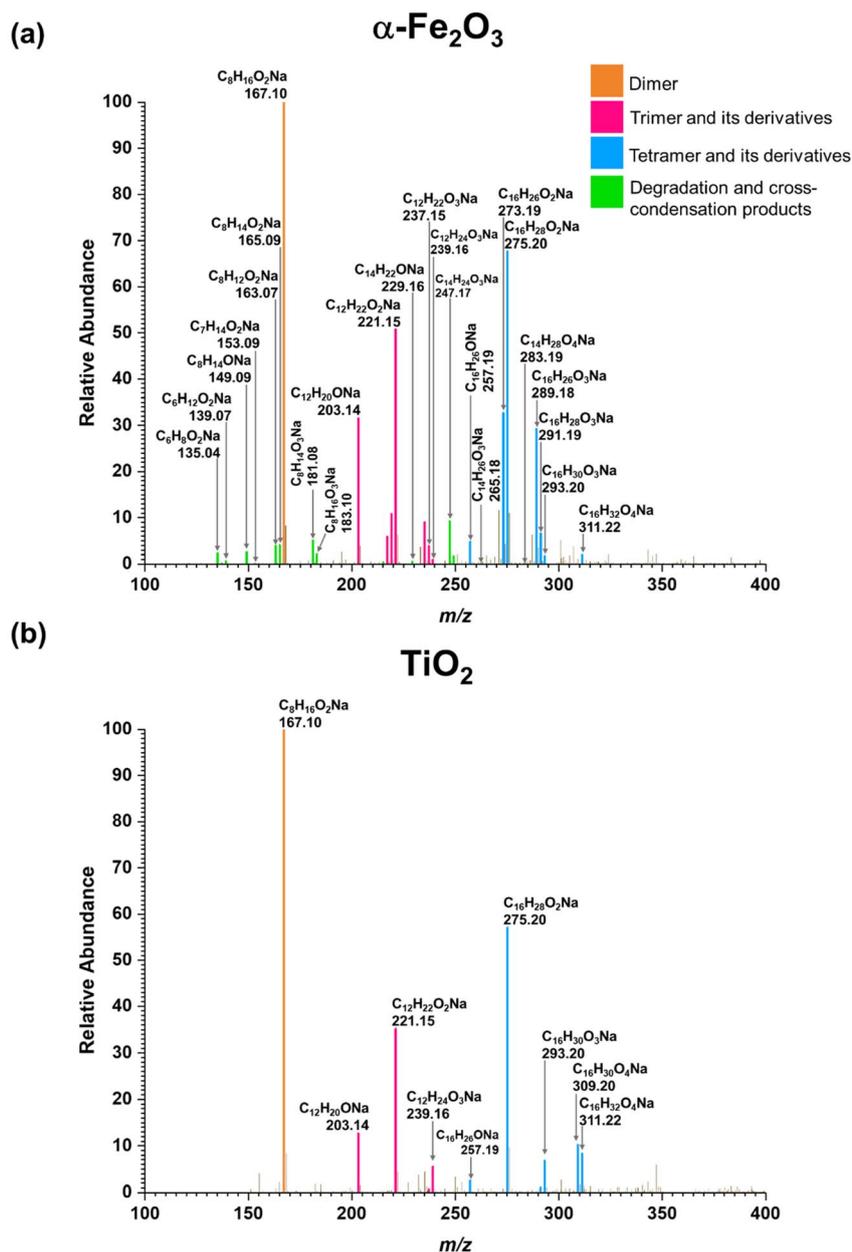
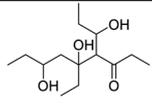**Fig. 7** HRMS patterns of surface products formed from the reaction of MEK with NO_2 on (a) α-Fe_2O_3 and (b) TiO_2 under dry conditions.

The formation of these compounds indicates that adsorbed MEK on α-Fe_2O_3 surfaces undergo a degradation process in the presence of NO_2 to produce acetaldehyde and formaldehyde, which is a well-known atmospheric reaction often considered to occur under photochemical conditions and/or in the presence of ozone.[19] NO_2 is an oxidizer and degradation of MEK by NO_2 is mediated on α-Fe_2O_3 surfaces, perhaps by adsorbed nitrate species. While neither acetaldehyde nor formaldehyde was identified in our experiments possibly due to lower m/z values, Compounds **9** and **10** are self-condensation products of acetaldehyde (Scheme 3). Compound **11** may be formed *via* cross-condensation of MEK with acet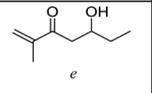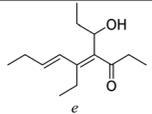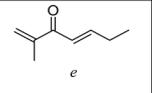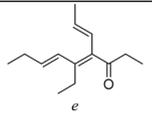aldehyde. However, **11** is a precursor for both **12** and **16**, and thus observed with lower relative intensity. The dimerization of **11** forms **12**, and subsequent dehydration products, **13**, **14**, and **15**. The structure of **14** was confirmed *via* MS/MS and, extended to its monomer, **11**. Briefly, for $m/z = 247.17$ to produce a fragment at 218.12, both **14** and **11** must be ethyl ketones. This structure will be possible only with the cross-condensation of MEK enolate with acetaldehyde (Scheme 3). The cross-condensation of **11** with formaldehyde forms **16**, along with its subsequent dehydration products, **17** and **18**. Furthermore, the m/z fragment at 165.09 for $C_8H_{14}O_2Na$ also forms during MS analysis due to the loss of 2H from the MEK dimer. However, for solvent-extracted samples of MEK-adsorbed α-Fe_2O_3, the ratio of relative intensities of 165.09/167.10 is 0.017 whereas that for NO_2-exposed

Table 3 MEK degradation and cross-condensation products identified on α-Fe$_2$O$_3$ surfaces after reactions with NO$_2$

Group D - Self-Condensation of acetaldehyde, and its derivatives	Group E - Cross-Condensation of acetaldehyde, its and derivatives		
	Sub Group E1 - Cross-Condensation of acetaldehyde with MEK	Sub Group E2 - Dimerization and dehydration products of 11	Sub Group E3 - Cross-Condensation of 11 with formaldehyde, and its dehydration products
Compound 9 139.07 [a] C$_6$H$_{12}$O$_2$Na [b] (C$_6$H$_{12}$O$_2$) [c]	Compound 11 [d] 153.09 C$_7$H$_{14}$O$_2$Na (C$_7$H$_{14}$O$_2$) [f]	Compound 12 [d] 283.19 C$_{14}$H$_{28}$O$_4$Na (C$_{14}$H$_{28}$O$_4$)	Compound 16 183.10 C$_8$H$_{16}$O$_3$Na (C$_8$H$_{16}$O$_3$)
Compound 10 [d] 121.05 C$_6$H$_{10}$ONa (C$_6$H$_{10}$O) [e]		Compound 13 [d] 265.18 C$_{14}$H$_{26}$O$_3$Na (C$_{14}$H$_{26}$O$_3$) [e]	Compound 17 165.09 [g] C$_8$H$_{14}$O$_2$Na (C$_8$H$_{14}$O$_2$) [e]
		Compound 14 247.17 C$_{14}$H$_{24}$O$_2$Na (C$_{14}$H$_{24}$O$_2$) [e]	Compound 18 [d] 147.08 C$_8$H$_{12}$ONa (C$_8$H$_{12}$O) [e]
		Compound 15 [d] 229.16 C$_{14}$H$_{22}$ONa (C$_{14}$H$_{22}$O) [e]	
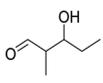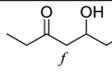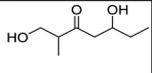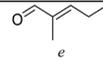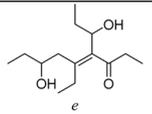
[a] : m/z. [b] : Observed formula. [c] : Molecular formula. [d] : Observed with trace quantities, within acceptable mass tolerance. [e] : C=C was assigned based on the most stable structure due to the formation of conjugated systems and/or MS/MS pattern. [f] : The structure was determined based on the MS/MS pattern of **14** due to the lower intensity of **11**. [g] : $m/z = 165.09$ also forms from MEK dimer ($m/z = 167.10$) due to the loss of 2H during analysis. Here, the ratio of 165.09/167.10 is higher compared to other systems with MEK dimer indicating a second source of formation.
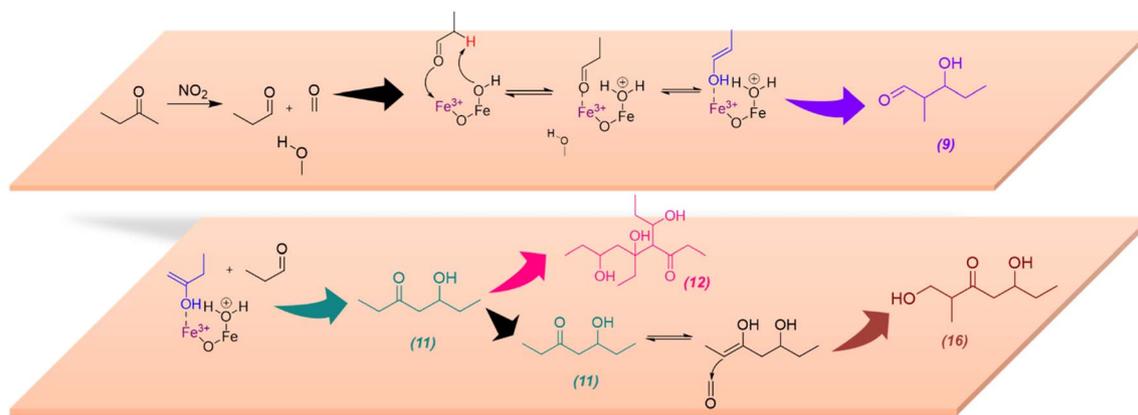
Scheme 3 Proposed mechanistic pathways for the formation of MEK degradation and cross-condensation products **9**, **11**, **12**, and **16** on α-Fe$_2$O$_3$ surfaces in the presence of NO$_2$ (g).

MEK-adsorbed α-Fe$_2$O$_3$ is 0.041, evidence of additional sources for the formation of the fragment at $m/z = 165.09$. Therefore, these results underscore the surface-specific SOA formation on mineral surfaces from common VOCs such as MEK in the presence of trace gas pollutants such as NO$_2$.

4   Conclusion

The adsorption of methyl ethyl ketone (MEK) on oxide surfaces, specifically α-Fe$_2$O$_3$ and TiO$_2$, yields MEK oligomers and their dehydration products. Similar oligomer formation chemistry was observed with authentic dust samples, Arizona Test Dust and Gobi Dust samples. These oligomers were primarily MEK dimer, MEK trimer, and MEK tetramer whereas these products do not form on SiO$_2$. The formation of these oligomers on mineral oxide surfaces involves reactions with surface hydroxyl groups as confirmed *via* isotope labeling experiments with deuteroxylated α-Fe$_2$O$_3$ and TiO$_2$ surfaces. In the presence of gas-phase water (80% RH), surface product speciation on α-Fe$_2$O$_3$ surfaces shifted toward high-molecular-weight oligomers and their dehydration

products, whereas for TiO_2, a slight increase in high-molecular-weight oligomers was identified. These results indicate the important role of water molecules in these surface-mediated oligomerization reactions that are mineral specific. Moreover, when MEK-adsorbed mineral surfaces were exposed to $NO_2(g)$, MEK degradation to acetaldehyde and formaldehyde on α-Fe_2O_3 surfaces followed by self- and cross-condensation was observed, underscoring the specific role of mineral surface.

Overall, this study shows how mineral dust aerosol surfaces can interact with atmospherically prevalent carbonyl compounds that are often regarded as too insignificant to be involved in heterogeneous and multiphase reactions to yield SOAs. Moreover, these compounds can be oxidized in the presence of nitrogen oxides. These data show that small carbonyl compounds interact with surfaces and undergo oligomerization reactions producing high-molecular-weight and oxygenated SOAs. Furthermore, water molecules in the atmosphere act as a catalyst/aid in catalyzing these surface-mediated reactions and stabilizing intermediates, thereby enhancing the formation of these larger oligomers on mineral surfaces that are mineral specific. Additionally, VOCs such as MEK can undergo surface-mediated degradation in the presence of NO_2, even under dark conditions irrespective of the availability of other common oxidants such as HO, ozone, or H_2O_2, thereby initiating additional aldol-condensation reactions on mineral surfaces. In the environment, VOCs such as MEK are ubiquitous, emitting from both natural and anthropogenic sources. During dust transport and urban dust episodes, these VOCs and trace gas pollutants such as NO_2 can interact with each other, forming SOAs that are more highly oxygenated and less volatile as shown here on these different mineral surfaces under different relative humidity. Further reactions of these oligomers formed from MEK with other atmospheric components may induce the formation of BrC, and this is an area worthy of additional study. This study suggests that heterogeneous reactions are possible pathways for oligomerization reactions of small organic compounds and the formation of various highly oxygenated SOAs. Furthermore, the adsorption of small carbonyl compounds on authentic dust such as Arizona Test Dust and natural dust samples show that these reactivities occur within these samples and on different mineral surfaces that make up these complex dust samples.

Author contribution

Conceptualization was jointly by VHG & EH; funding acquisition, supervision, and project administration were carried out by VHG; investigation, data curation, formal analysis, validation, and writing the original draft of the manuscript were carried out by EH; reviewing and editing of the manuscript were performed jointly by VHG & EH.

Conflicts of interest

All authors declare no competing interests.

References

1 H. O. T. Pye, C. K. Ward-Caviness, B. N. Murphy, K. W. Appel and K. M. Seltzer, Secondary organic aerosol association with cardiorespiratory disease mortality in the United States, *Nat. Commun.*, 2021, **12**, 7215.

2 J. Liu, B. Chu, T. Chen, C. Zhong, C. Liu, Q. Ma, J. Ma, P. Zhang and H. He, Secondary Organic Aerosol Formation Potential from Ambient Air in Beijing: Effects of Atmospheric Oxidation Capacity at Different Pollution Levels, *Environ. Sci. Technol.*, 2021, **55**, 4565–4572.

3 C. Wong, D. Vite and S. A. Nizkorodov, Stability of α-Pinene and d -Limonene Ozonolysis Secondary Organic Aerosol Compounds Toward Hydrolysis and Hydration, *ACS Earth Space Chem.*, 2021, **5**, 2555–2564.

4 F. Khan, K. Kwapiszewska, Y. Zhang, Y. Chen, A. T. Lambe, A. Kołodziejczyk, N. Jalal, K. Rudzinski, A. Martínez-Romero, R. C. Fry, J. D. Surratt and R. Szmigielski, Toxicological Responses of α-Pinene-Derived Secondary Organic Aerosol and Its Molecular Tracers in Human Lung Cell Lines, *Chem. Res. Toxicol.*, 2021, **34**, 817–832.

5 S. Ge, G. Wang, S. Zhang, D. Li, Y. Xie, C. Wu, Q. Yuan, J. Chen and H. Zhang, Abundant NH_3 in China Enhances Atmospheric HONO Production by Promoting the Heterogeneous Reaction of SO_2 with NO_2, *Environ. Sci. Technol.*, 2019, **53**, 14339–14347.

6 S. A. Mang, D. K. Henricksen, A. P. Bateman, M. P. S. Andersen, D. R. Blake and S. A. Nizkorodov, Contribution of Carbonyl Photochemistry to Aging of Atmospheric Secondary Organic Aerosol, *J. Phys. Chem. A*, 2008, **112**, 8337–8344.

7 D. Srivastava, T. V. Vu, S. Tong, Z. Shi and R. M. Harrison, Formation of secondary organic aerosols from anthropogenic precursors in laboratory studies, *npj Clim. Atmos. Sci.*, 2022, **5**, 22.

8 B. Ervens and S. M. Kreidenweis, SOA Formation by Biogenic and Carbonyl Compounds: Data Evaluation and Application, *Environ. Sci. Technol.*, 2007, **41**, 3904–3910.

9 Q. Liu, Y. Gao, W. Huang, Z. Ling, Z. Wang and X. Wang, Carbonyl compounds in the atmosphere: A review of abundance, source and their contributions to O_3 and SOA formation, *Atmos. Res.*, 2022, **274**, 106184.

10 M. Kalberer, D. Paulsen, M. Sax, M. Steinbacher, J. Dommen, A. S. H. Prevot, R. Fisseha, E. Weingartner, V. Frankevich, R. Zenobi and U. Baltensperger, Identification of Polymers as Major Components of Atmospheric Organic Aerosols, *Science*, 2004, **303**, 1659–1662.

11 J. F. Brewer, E. V. Fischer, R. Commane, S. C. Wofsy, B. C. Daube, E. C. Apel, A. J. Hills, R. S. Hornbrook, B. Barletta, S. Meinardi, D. R. Blake, E. A. Ray and A. R. Ravishankara, Evidence for an Oceanic Source of

Methyl Ethyl Ketone to the Atmosphere, *Geophys. Res. Lett.*, 2020, **47**(4), e2019GL086045.

12 H. Shen, Z. Chen, H. Li, X. Qian, X. Qin and W. Shi, Gas-Particle Partitioning of Carbonyl Compounds in the Ambient Atmosphere, *Environ. Sci. Technol.*, 2018, **52**, 10997–11006.

13 G. T. Drozd, K. S.-M. Brown and H. Q. Karp, Effects of Organic Matrices on Nucleophilic Aqueous Aerosol Chemistry: Yields and Mechanistic Insight for Brown Carbon Formation from Glyoxal and Ammonia, *ACS Earth Space Chem.*, 2022, **6**, 1772–1781.

14 S. Tang, F. Li, J. Lv, L. Liu, G. Wu, Y. Wang, W. Yu, Y. Wang and G. Jiang, Unexpected molecular diversity of brown carbon formed by Maillard-like reactions in aqueous aerosols, *Chem. Sci.*, 2022, **13**, 8401–8411.

15 R. Zhang, M. Gen, Z. Liang, Y. J. Li and C. K. Chan, Photochemical Reactions of Glyoxal during Particulate Ammonium Nitrate Photolysis: Brown Carbon Formation, Enhanced Glyoxal Decay, and Organic Phase Formation, *Environ. Sci. Technol.*, 2022, **56**, 1605–1614.

16 N. G. Jimenez, K. D. Sharp, T. Gramyk, D. Z. Ugland, M.-K. Tran, A. Rojas, M. A. Rafla, D. Stewart, M. M. Galloway, P. Lin, A. Laskin, M. Cazaunau, E. Pangui, J. F. Doussin and D. O. De Haan, Radical-Initiated Brown Carbon Formation in Sunlit Carbonyl–Amine–Ammonium Sulfate Mixtures and Aqueous Aerosol Particles, *ACS Earth Space Chem.*, 2022, **6**, 228–238.

17 K. M. Updyke, T. B. Nguyen and S. A. Nizkorodov, Formation of brown carbon via reactions of ammonia with secondary organic aerosols from biogenic and anthropogenic precursors, *Atmos. Environ.*, 2012, **63**, 22–31.

18 J. F. Brewer, D. K. Papanastasiou, J. B. Burkholder, E. V. Fischer, Y. Ren, A. Mellouki and A. R. Ravishankara, Atmospheric Photolysis of Methyl Ethyl, Diethyl, and Propyl Ethyl Ketones: Temperature-Dependent UV Absorption Cross Sections, *J. Geophys. Res.: Atmos.*, 2019, **124**, 5906–5918.

19 A. M. Yáñez-Serrano, A. C. Nölscher, E. Bourtsoukidis, B. Derstroff, N. Zannoni, V. Gros, M. Lanza, J. Brito, S. M. Noe, E. House, C. N. Hewitt, B. Langford, E. Nemitz, T. Behrendt, J. Williams, P. Artaxo, M. O. Andreae and J. Kesselmeier, Atmospheric mixing ratios of methyl ethyl ketone (2-butanone) in tropical, boreal, temperate and marine environments, *Atmos. Chem. Phys.*, 2016, **16**, 10965–10984.

20 B. Davison, A. Brunner, C. Ammann, C. Spirig, M. Jocher and A. Neftel, Cut-induced VOC emissions from agricultural grasslands, *Plant Biol.*, 2008, **10**, 76–85.

21 K. A. McKinney, B. H. Lee, A. Vasta, T. V. Pho and J. W. Munger, Emissions of isoprenoids and oxygenated biogenic volatile organic compounds from a New England mixed forest, *Atmos. Chem. Phys.*, 2011, **11**, 4807–4831.

22 T. M. Ruuskanen, M. Müller, R. Schnitzhofer, T. Karl, M. Graus, I. Bamberger, L. Hörtnagl, F. Brilli, G. Wohlfahrt and A. Hansel, Eddy covariance VOC emission and deposition fluxes above grassland using PTR-TOF, *Atmos. Chem. Phys.*, 2011, **11**, 611–625.

23 G. Song and C.-M. Ryu, Two Volatile Organic Compounds Trigger Plant Self-Defense against a Bacterial Pathogen and a Sucking Insect in Cucumber under Open Field Conditions, *Int. J. Mol. Sci.*, 2013, **14**, 9803–9819.

24 A. Tani, K. Muramatsu and T. Mochizuki, Emission of Methyl Ethyl Ketone and 2-Butanol Converted from Methyl Vinyl Ketone in Plant Leaves, *Atmosphere*, 2020, **11**, 793.

25 M. O. Andreae and P. Merlet, Emission of trace gases and aerosols from biomass burning, *Global Biogeochem. Cycles*, 2001, **15**, 955–966.

26 S. Kim, S.-Y. Kim, M. Lee, H. Shim, G. M. Wolfe, A. B. Guenther, A. He, Y. Hong and J. Han, Impact of isoprene and HONO chemistry on ozone and OVOC formation in a semirural South Korean forest, *Atmos. Chem. Phys.*, 2015, **15**, 4357–4371.

27 D. M. Bon, I. M. Ulbrich, J. A. de Gouw, C. Warneke, W. C. Kuster, M. L. Alexander, A. Baker, A. J. Beyersdorf, D. Blake, R. Fall, J. L. Jimenez, S. C. Herndon, L. G. Huey, W. B. Knighton, J. Ortega, S. Springston and O. Vargas, Measurements of volatile organic compounds at a suburban ground site (T1) in Mexico City during the MILAGRO 2006 campaign: measurement comparison, emission ratios, and source attribution, *Atmos. Chem. Phys.*, 2011, **11**, 2399–2421.

28 J. Brito, F. Wurm, A. M. Yáñez-Serrano, J. V. de Assunção, J. M. Godoy and P. Artaxo, Vehicular Emission Ratios of VOCs in a Megacity Impacted by Extensive Ethanol Use: Results of Ambient Measurements in São Paulo, Brazil, *Environ. Sci. Technol.*, 2015, **49**, 11381–11387.

29 J. de Gouw and C. Warneke, Measurements of volatile organic compounds in the earth's atmosphere using proton-transfer-reaction mass spectrometry, *Mass Spectrom. Rev.*, 2007, **26**, 223–257.

30 R. Sommariva, J. A. de Gouw, M. Trainer, E. Atlas, P. D. Goldan, W. C. Kuster, C. Warneke and F. C. Fehsenfeld, Emissions and photochemistry of oxygenated VOCs in urban plumes in the Northeastern United States, *Atmos. Chem. Phys.*, 2011, **11**, 7081–7096.

31 P. Li, K. A. Perreau, E. Covington, C. H. Song, G. R. Carmichael and V. H. Grassian, Heterogeneous reactions of volatile organic compounds on oxide particles of the most abundant crustal elements: Surface reactions of acetaldehyde, acetone, and propionaldehyde on SiO_2, Al_2O_3, Fe_2O_3, TiO_2, and CaO, *J. Geophys. Res.: Atmos.*, 2001, **106**, 5517–5529.

32 M. El-Maazawi, A. N. Finken, A. B. Nair and V. H. Grassian, Adsorption and Photocatalytic Oxidation of Acetone on TiO2: An in Situ Transmission FT-IR Study, *J. Catal.*, 2000, **191**, 138–146.

33 Y. Li, Y. Ji, J. Zhao, Y. Wang, Q. Shi, J. Peng, Y. Wang, C. Wang, F. Zhang, Y. Wang, J. H. Seinfeld and R. Zhang, Unexpected Oligomerization of Small α-Dicarbonyls for Secondary Organic Aerosol and Brown Carbon Formation, *Environ. Sci. Technol.*, 2021, **55**, 4430–4439.

34 M. Jang and R. M. Kamens, Atmospheric Secondary Aerosol Formation by Heterogeneous Reactions of Aldehydes in the

© 2023 The Author(s). Published by the Royal Society of Chemistry

Environ. Sci.: Atmos., 2023, **3**, 799–815 | 813

Presence of a Sulfuric Acid Aerosol Catalyst, *Environ. Sci. Technol.*, 2001, **35**, 4758–4766.

35 M. Hajaghazadeh, V. Vaiano, D. Sannino, H. Kakooei, R. Sotudeh-Gharebagh and P. Ciambelli, Heterogeneous photocatalytic oxidation of methyl ethyl ketone under UV-A light in an LED-fluidized bed reactor, *Catal. Today*, 2014, **230**, 79–84.

36 C. Knote, A. Hodzic, J. L. Jimenez, R. Volkamer, J. J. Orlando, S. Baidar, J. Brioude, J. Fast, D. R. Gentner, A. H. Goldstein, P. L. Hayes, W. B. Knighton, H. Oetjen, A. Setyan, H. Stark, R. Thalman, G. Tyndall, R. Washenfelder, E. Waxman and Q. Zhang, Simulation of semi-explicit mechanisms of SOA formation from glyoxal in aerosol in a 3-D model, *Atmos. Chem. Phys.*, 2014, **14**, 6213–6239.

37 T.-M. Fu, D. J. Jacob, F. Wittrock, J. P. Burrows, M. Vrekoussis and D. K. Henze, Global budgets of atmospheric glyoxal and methylglyoxal, and implications for formation of secondary organic aerosols, *J. Geophys. Res.*, 2008, **113**, D15303.

38 M. Jang, N. M. Czoschke, S. Lee and R. M. Kamens, Heterogeneous Atmospheric Aerosol Production by Acid-Catalyzed Particle-Phase Reactions, *Science*, 2002, **298**, 814–817.

39 R. Volkamer, F. San Martini, L. T. Molina, D. Salcedo, J. L. Jimenez and M. J. Molina, A missing sink for gas-phase glyoxal in Mexico City: Formation of secondary organic aerosol, *Geophys. Res. Lett.*, 2007, **34**, L19807.

40 Y. Ji, Q. Shi, X. Ma, L. Gao, J. Wang, Y. Li, Y. Gao, G. Li, R. Zhang and T. An, Elucidating the critical oligomeric steps in secondary organic aerosol and brown carbon formation, *Atmos. Chem. Phys.*, 2022, **22**, 7259–7271.

41 D. Grosjean, E. Grosjean and L. F. R. Moreira, Speciated Ambient Carbonyls in Rio de Janeiro, Brazil, *Environ. Sci. Technol.*, 2002, **36**, 1389–1395.

42 P. Pinho, C. Pio and M. Jenkin, Evaluation of isoprene degradation in the detailed tropospheric chemical mechanism, MCM v3, using environmental chamber data, *Atmos. Environ.*, 2005, **39**, 1303–1322.

43 K. Kandler, N. Benker, U. Bundke, E. Cuevas, M. Ebert, P. Knippertz, S. Rodríguez, L. Schütz and S. Weinbruch, Chemical Composition and Complex Refractive Index of Saharan Mineral Dust at Izaña, Tenerife (Spain) Derived by Electron Microscopy, *Atmos. Environ.*, 2007, **41**, 8058–8074.

44 G. Rubasinghege and V. H. Grassian, Role(s) of adsorbed water in the surface chemistry of environmental interfaces, *Chem. Commun.*, 2013, **49**, 3071.

45 Z. Bozkurt, Ö. Ö. Üzmez, T. Döğeroğlu, G. Artun and E. O. Gaga, Atmospheric concentrations of SO_2, NO_2, ozone and VOCs in Düzce, Turkey using passive air samplers: Sources, spatial and seasonal variations and health risk estimation, *Atmos. Pollut. Res.*, 2018, **9**, 1146–1156.

46 L. Pinault, D. Crouse, M. Jerrett, M. Brauer and M. Tjepkema, Spatial associations between socioeconomic groups and NO_2 air pollution exposure within three large Canadian cities, *Environ. Res.*, 2016, **147**, 373–382.

47 C. E. Nanayakkara, W. A. Larish and V. H. Grassian, Titanium Dioxide Nanoparticle Surface Reactivity with Atmospheric Gases, CO_2, SO_2, and NO_2: Roles of Surface Hydroxyl Groups and Adsorbed Water in the Formation and Stability of Adsorbed Products, *J. Phys. Chem. C*, 2014, **118**, 23011–23021.

48 M. Tang, W. A. Larish, Y. Fang, A. Gankanda and V. H. Grassian, Heterogeneous Reactions of Acetic Acid with Oxide Surfaces: Effects of Mineralogy and Relative Humidity, *J. Phys. Chem. A*, 2016, **120**, 5609–5616.

49 Y. Fang, M. Tang and V. H. Grassian, Competition between Displacement and Dissociation of a Strong Acid Compared to a Weak Acid Adsorbed on Silica Particle Surfaces: The Role of Adsorbed Water, *J. Phys. Chem. A*, 2016, **120**, 4016–4024.

50 Y. Fang, D. Lesnicki, K. J. Wall, M. P. Gaigeot, M. Sulpizi, V. Vaida and V. H. Grassian, Heterogeneous Interactions between Gas-Phase Pyruvic Acid and Hydroxylated Silica Surfaces: A Combined Experimental and Theoretical Study, *J. Phys. Chem. A*, 2019, **123**, 983–991.

51 A. L. Goodman, E. T. Bernard and V. H. Grassian, Spectroscopic Study of Nitric Acid and Water Adsorption on Oxide Particles: Enhanced Nitric Acid Uptake Kinetics in the Presence of Adsorbed Water, *J. Phys. Chem. A*, 2001, **105**, 6443–6457.

52 E. Hettiarachchi and V. H. Grassian, Heterogeneous Formation of Organonitrates (ON) and Nitroxy-Organosulfates (NOS) from Adsorbed α-Pinene-Derived Organosulfates (OS) on Mineral Surfaces, *ACS Earth Space Chem.*, 2022, **6**, 3017–3030.

53 C. E. Nanayakkara, J. Pettibone and V. H. Grassian, Sulfur dioxide adsorption and photooxidation on isotopically-labeled titanium dioxide nanoparticle surfaces: Roles of surface hydroxyl groups and adsorbed water in the formation and stability of adsorbed sulfite and sulfate, *Phys. Chem. Chem. Phys.*, 2012, **14**, 6957–6966.

54 J. Baltrusaitis and V. H. Grassian, Surface Reactions of Carbon Dioxide at the Adsorbed Water–Iron Oxide Interface, *J. Phys. Chem. B*, 2005, **109**, 12227–12230.

55 G. M. Underwood, P. Li, H. Al-Abadleh and V. H. Grassian, A Knudsen Cell Study of the Heterogeneous Reactivity of Nitric Acid on Oxide and Mineral Dust Particles, *J. Phys. Chem. A*, 2001, **105**, 6609–6620.

56 G. Socrates, *Infrared and Raman Characteristic Group Frequencies*, Wiley, 3rd edn, 2000.

57 *Methyl Ethyl Ketone – NIST*, **https://webbook.nist.gov/cgi/cbook.cgi?Spec=C78933&Index=12&Type=IR&Large=on&SVG=on**, (accessed 5 December 2022).

58 E. S. Frank, H. Fan, M. Shrestha, S. Riahi, D. J. Tobias and V. H. Grassian, Impact of Adsorbed Water on the Interaction of Limonene with Hydroxylated SiO_2: Implications of π-Hydrogen Bonding for Surfaces in Humid Environments, *J. Phys. Chem. A*, 2020, **124**, 10592–10599.

59 K. Hadjiivanov, in *Advances in Catalysis*, 2014, pp. 99–318.

60 R. A. Hancock, B. S. Thyagarajan and R. Walder, Chemical ionization mass spectrometry: Oligomerization reactions in tight ion sources, *Org. Mass Spectrom.*, 1980, **15**, 101–104.

61 D. M. Griffiths and C. H. Rochester, Infrared study of the adsorption of acetone on rutile, *J. Chem. Soc., Faraday Trans. 1*, 1978, **74**, 403.

62 A. Panov and J. J. Fripiat, An Infrared Spectroscopic Study of Acetone and Mesityl Oxide Adsorption on Acid Catalyst, *Langmuir*, 1998, **14**, 3788–3796.

63 J. Liggio and S.-M. Li, Reactive uptake of pinonaldehyde on acidic aerosols, *J. Geophys. Res.*, 2006, **111**, D24303.

64 P. Renard, S. Tlili, S. Ravier, E. Quivet and A. Monod, Aqueous phase oligomerization of α,β-unsaturated carbonyls and acids investigated using ion mobility spectrometry coupled to mass spectrometry (IMS-MS), *Atmos. Environ.*, 2016, **130**, 153–162.

65 Y. Liu, F. Siekmann, P. Renard, A. El Zein, G. Salque, I. El Haddad, B. Temime-Roussel, D. Voisin, R. Thissen and A. Monod, Oligomer and SOA formation through aqueous phase photooxidation of methacrolein and methyl vinyl ketone, *Atmos. Environ.*, 2012, **49**, 123–129.

66 P. Renard, F. Siekmann, G. Salque, C. Demelas, B. Coulomb, L. Vassalo, S. Ravier, B. Temime-Roussel, D. Voisin and A. Monod, Aqueous-phase oligomerization of methyl vinyl ketone through photooxidation – Part 1: Aging processes of oligomers, *Atmos. Chem. Phys.*, 2015, **15**, 21–35.

67 J. Clayden, N. Greeves and S. Warren, *Organic Chemistry*, New York: Oxford University Press, 2nd edn, 2012.

68 H. Metiu, S. Chrétien, Z. Hu, B. Li and X. Sun, Chemistry of Lewis Acid–Base Pairs on Oxide Surfaces, *J. Phys. Chem. C*, 2012, **116**, 10439–10450.

69 G. Alagona, C. Ghio and P. I. Nagy, The catalytic effect of water on the keto–enol tautomerism. Pyruvate and acetylacetone: a computational challenge, *Phys. Chem. Chem. Phys.*, 2010, **12**, 10173.

70 A. Datar, H. Paithankar, P. Deb, J. Chugh, S. Bagchi, A. Mukherjee and A. Hazra, Water-Controlled Keto–Enol Tautomerization of a Prebiotic Nucleobase, *J. Phys. Chem. B*, 2022, **126**, 5735–5743.

71 S. Yamabe, N. Tsuchida and K. Miyajima, Reaction Paths of Keto−Enol Tautomerization of β-Diketones, *J. Phys. Chem. A*, 2004, **108**, 2750–2757.

72 X. Jin, D. Wu, C. Liu, S. Huang, Z. Zhou, H. Wu, X. Chen, M. Huang, S. Zhou and C. Gu, Facet effect of hematite on the hydrolysis of phthalate esters under ambient humidity conditions, *Nat. Commun.*, 2022, **13**, 6125.

73 T. Zheng, C. Wu, M. Chen, Y. Zhang and P. T. Cummings, A DFT study of water adsorption on rutile TiO 2 (110) surface: The effects of surface steps, *J. Chem. Phys.*, 2016, **145**, 044702.

74 F. Jones, A. L. Rohl, J. B. Farrow and W. van Bronswijk, Molecular modeling of water adsorption on hematite, *Phys. Chem. Chem. Phys.*, 2000, **2**, 3209–3216.

75 C. A. Morrow, D. E. Moore and D. A. Lockner, The effect of mineral bond strength and adsorbed water on fault gouge frictional strength, *Geophys. Res. Lett.*, 2000, **27**, 815–818.

76 M. Sulpizi, M.-P. Gaigeot and M. Sprik, The Silica–Water Interface: How the Silanols Determine the Surface Acidity and Modulate the Water Properties, *J. Chem. Theory Comput.*, 2012, **8**, 1037–1047.

77 Y. Fang, P. S. J. Lakey, S. Riahi, A. T. McDonald, M. Shrestha, D. J. Tobias, M. Shiraiwa and V. H. Grassian, A molecular picture of surface interactions of organic compounds on prevalent indoor surfaces: Limonene adsorption on SiO2, *Chem. Sci.*, 2019, **10**, 2906–2914.

© 2023 The Author(s). Published by the Royal Society of Chemistry

Environ. Sci.: Atmos., 2023, **3**, 799–815 | **815**